

Piezoelectric properties of ferroelectric perovskite superlattices with polar discontinuity

Alexander I. Lebedev*

Physics Department, Moscow State University, 119991 Moscow, Russia

(Dated: December 17, 2020)

The stability of a high-symmetry $P4mm$ polar phase in seventeen short-period ferroelectric perovskite superlattices with polar discontinuity is studied from first principles within the density-functional theory. It is shown that in most superlattices this phase exhibits either the ferroelectric instability or the antiferrodistortive one, or both of them. For each superlattice, the ground-state structure, the structure of possible metastable phases, the spontaneous polarization, and piezoelectric properties are calculated. The properties of superlattices with the polar discontinuity are compared with those of superlattices with broken symmetry and of ordinary superlattices, which have no the polar discontinuity. It is shown that high piezoelectric coefficients (up to 150–270 pC/N) in some superlattices with the polar discontinuity are due to the appearance of strong lattice distortions, whose symmetry follows that of a low-lying polar phonon mode of the ground-state structure, under the influence of external strain.

DOI: 10.1016/j.commatsci.2020.110113

Keywords: ferroelectric superlattices, piezoelectricity, phase transitions, polar discontinuity, perovskites

I. INTRODUCTION

In recent years, much attention has been paid to studies of low-dimensional structures in which new physical phenomena that have no analogues in bulk materials have been discovered. Due to these new functional properties, these materials are considered as very promising for their use in electronics. Ferroelectric superlattices (SLs)—quasi-two-dimensional artificial periodic structures whose properties can be tailored to obtain the necessary functionality—belong to this interesting class of materials.

Most of the earlier experimental [1–23] and theoretical [24–48] studies of ferroelectric superlattices with the perovskite structure were performed on II-IV/II-IV or I-V/I-V type superlattices (here, the numbers indicate the valence of atoms entering the A and B sites of the ABO_3 perovskite structure). In such superlattices, there are no double electric layers at the interface between two dielectric materials, and therefore both the bulk and interfaces of these superlattices remain macroscopically electrically neutral.

Studies of the $\text{SrTiO}_3/\text{LaAlO}_3$ heterostructures have revealed new interesting phenomena that appear in these structures as a result of so-called polar discontinuity—of a polarization jump induced by effective $\pm e/2$ charges per unit cell which appear at the interface between SrTiO_3 and LaAlO_3 because the charged character of LaO^+ and AlO_2^- layers [49]. These phenomena include the appearance of a conducting layer near the interface (a two-dimensional electron gas), its magnetism, and even superconductivity [49–51]. These phenomena can be controlled using an external electric field [52]. The divergence of the electrostatic potential in such heterostruc-

tures, which can result in the appearance of conductive layers at the interface between two dielectrics, is called a polar catastrophe. The possibility of the appearance of the two-dimensional electron gas at the interface between a ferroelectric and a nonpolar dielectric in perovskites was systematically studied in [53]. Later it was realized that conductive layers can also be obtained in ferroelectric structures without the polar discontinuity [54]. This made it possible to create new types of electronic devices—ferroelectric structures with switchable giant tunneling conductivity [55, 56]; the idea of such devices was proposed earlier in [57, 58]. Note that the appearance of similar phenomena can also be anticipated in epitaxial films of II-IV and I-V perovskites, which are grown on DyScO_3 , GdScO_3 , NdScO_3 , NdGaO_3 , and LaGaO_3 substrates to create a biaxial strain in them, since the polar discontinuity is possible in these structures [59].

Until now, theoretical studies of superlattices with the polar discontinuity have focused on studying the distribution of polarization and electric field in these structures and on finding the conditions for the appearance of a two-dimensional electron gas at the interface [59–70]. The questions of the stability of the high-symmetry polar structure in such SLs, possible phase transitions in them, and the physical properties of low-symmetry phases were not analyzed. At the same time, the ferroelectric and antiferrodistortive (AFD) instabilities characteristic of many perovskites can result in strong distortions of the structure of SLs. This means that the earlier predictions of their physical properties obtained without taking these distortions into account may be incorrect.

One of the questions that remains insufficiently studied is the question about the piezoelectric properties of superlattices with the polar discontinuity. The calculations of these properties are limited to the calculations for the high-symmetry tetragonal $P4mm$ phase of such

* swan@scon155.phys.msu.ru

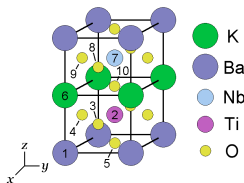


FIG. 1. Geometry of a typical superlattice.

SLs [71, 72]. It is known that the record-high piezoelectric properties of PbTiO_3 -based solid solutions near the morphotropic boundary [73] are due to the ease of inclination of the polarization vector from the [100] direction to the [111] one under the influence of the electric field [74] or mechanical stress. The polar discontinuity in SLs allows, under certain conditions, to obtain high values of irreversible polarization in their structures. This is why it was interesting to check whether it is possible to get high piezoelectric coefficients in superlattices with the polar discontinuity using the strain-induced inclination of the polarization vector. In Ref. [71], SLs with the polar discontinuity were already considered as a way to obtain stable, weakly temperature-dependent piezoelectric properties.

II. CALCULATION TECHNIQUE

In this work, the properties of seventeen free-standing [001]-oriented short-period II-IV/I-V, II-IV/III-III, and I-V/III-III superlattices with the polar discontinuity and a thickness of individual layers of one unit cell are studied from first principles. For comparison, similar calculations are performed for several superlattices with broken symmetry. The latter SLs have no the polar discontinuity, but their high-symmetry polar structure is formed by a sequence of layers with no mirror symmetry. In addition, the obtained results are compared with the results for ordinary superlattices with the mirror symmetry of the layer sequence. The geometry of the superlattices is shown in Fig. 1.

The choice of free-standing superlattices for our study stems from the fact that, when any coherently strained short-period superlattice is grown on a substrate, a transition layer containing misfit dislocations and other defects with a thickness of ~ 100 Å appears at the interface as a result of a mismatch between the equilibrium in-plane lattice parameter of the SL and that of the substrate. In the defect-free part of the superlattice, the in-plane lattice parameter relaxes to the lattice parameter of the free-standing superlattice. This is why in the majority of rather thick experimentally grown superlattices, the in-plane lattice parameter is close to that of free-standing superlattices.

First-principles calculations were performed within the density functional theory using the ABINIT program [75] and norm-conserving pseudopotentials constructed ac-

ording to the RRKJ scheme [76] in the local density approximation (LDA), like in [77]. The cutoff energy was 30 Ha (816 eV) with the exception of Ta-containing systems in which it was 40 Ha (1088 eV). Integration over the Brillouin zone was carried out using a $8 \times 8 \times 4$ Monkhorst–Pack mesh for high-symmetry structures and meshes with equivalent density of \mathbf{k} -points for low-symmetry phases. The equilibrium lattice parameters and atomic positions were calculated by relaxing forces acting on the atoms to values less than $2 \cdot 10^{-6}$ Ha/Bohr (0.1 meV/Å). The phonon spectra, the tensors of piezoelectric stress coefficients $e_{i\mu}$, and the elastic compliance tensors $S_{\mu\nu}$ were calculated using the density-functional perturbation theory. The $e_{i\mu}$ values were then converted to the piezoelectric strain coefficients $d_{i\nu}$ using the formula $d_{i\nu} = e_{i\mu} S_{\mu\nu}$, and for monoclinic structures the tensor components were transformed to the standard setting of the monoclinic unit cell, in which the polarization vector lies in the xz plane.

III. RESULTS AND DISCUSSION

1. Search for the ground-state structure

It is known that the electrical conductivity of materials is usually a factor that prevents the practical use of their ferroelectric properties. Since the experiments on structures with the polar discontinuity often revealed metallic conductivity at the interface, it was necessary first to ensure that the superlattices under study are insulating. The calculations confirmed that in all superlattices studied in the work, the conduction band is separated from the valence band by a sufficiently large energy gap (see Table S1 in the Supplementary data), and therefore all studied SLs are dielectrics.

Since the layer sequence in considered superlattices does not admit the reversal of $z \rightarrow -z$ (Fig. 1), the superlattices are always polar and their high-symmetry phase is described by the $P4mm$ space group. However, this structure can exhibit various instabilities characteristic of crystals with the perovskite structure: either the ferroelectric instability or the antiferrodistortive one, or both of them simultaneously. In this work, the ground state of superlattices was searched in the traditional way [38, 39]. First, the structures resulting from the condensation of all unstable phonons found in the phonon spectrum of the $P4mm$ phase were calculated taking into account a possible degeneracy of phonon modes. Then, by calculating the phonon frequencies at all high-symmetry points of the Brillouin zone and the elastic tensor for these distorted structures, the stability of the obtained solutions was checked. In the case when an instability was found in any of these structures, the search for the ground state was continued until a structure whose phonon spectrum has no unstable modes and whose matrix composed of the elastic tensor components in the Voigt notation is positive definite is found. In this case, the conclusion that a

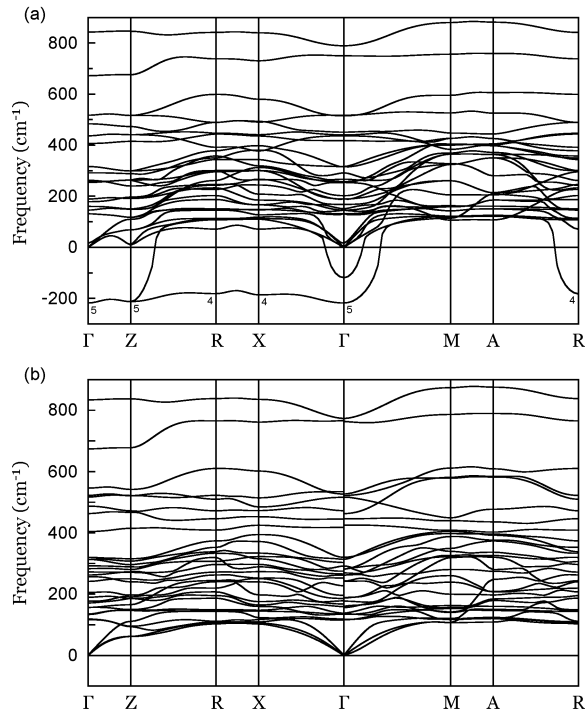


FIG. 2. Phonon spectrum of the $\text{KNbO}_3/\text{BaTiO}_3$ superlattice (a) in the high-symmetry $P4mm$ phase and (b) in the ground-state Cm phase. The numbers near the curves indicate the symmetry of unstable modes.

stable phase which can be a possible ground-state structure can be made. The problem here is that in chains of phases generated by different octahedra rotations, several stable states can be found, as was recently demonstrated for SrTiO_3 [78]. In this case, the ground state is the stable phase with the lowest total energy; other stable phases should be considered as metastable. If the energy of such metastable solutions differs little from the energy of the ground state, then these solutions should be considered as phases that can be observed in experiment. For them, as well as for the ground state, an analysis of their physical properties should also be carried out.

Calculations of the phonon spectra show that in most studied superlattices with the polar discontinuity (except for $\text{BaTiO}_3/\text{LaAlO}_3$, $\text{SrTiO}_3/\text{LaAlO}_3$, $\text{PbTiO}_3/\text{KTaO}_3$, $\text{PbTiO}_3/\text{LaAlO}_3$, and $\text{KTaO}_3/\text{LaAlO}_3$) the high-symmetry $P4mm$ phase exhibits the ferroelectric instability with respect to the in-plane distortion of the structure or, in other words, to the inclination of the polarization vector. The phonon spectrum of one of such superlattices, $\text{KNbO}_3/\text{BaTiO}_3$, is shown in Fig. 2. It is seen that in addition to the instability at the Γ point, the instabilities also appear at the X , R , and Z points of the Brillouin zone. We have already encountered a similar situation in $\text{KNbO}_3/\text{KTaO}_3$ [42] and $\text{BaTiO}_3/\text{BaZrO}_3$ [44] SLs.

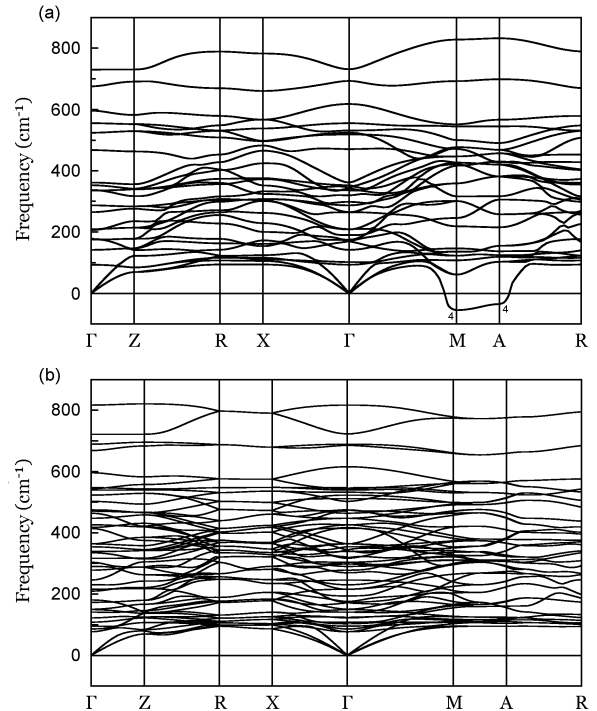


FIG. 3. Phonon spectrum of the $\text{BaTiO}_3/\text{LaAlO}_3$ superlattice (a) in the high-symmetry $P4mm$ phase and (b) in the ground-state $P4bm$ phase. The numbers near the curves indicate the symmetry of unstable modes.

An instability zone, which is observed as a band of imaginary phonon frequencies on the Γ - Z - R - X - Γ line (imaginary frequencies are represented in the figure by negative values), is a consequence of the ferroelectric instability in the $\dots\text{-Ti-O}\dots$ chains propagating in the plane of the SL—the so-called chain instability [79]. Indeed, an analysis of the eigenvectors of these modes shows that at all the above-mentioned points of the Brillouin zone the out-of-phase, transverse, xy -polarized displacements of Ti and O atoms in chains propagating in the $[100]$ and $[010]$ directions dominate in the atomic motion. In $\text{Ba}(\text{Sr})\text{TiO}_3/\text{KNb}(\text{Ta})\text{O}_3$ superlattices, the displacements of the Nb(Ta) atoms are small, whereas in superlattices containing no Ti atoms as well as in the $\text{PbTiO}_3/\text{KNbO}_3$ SL the chain instability is observed mainly in $\dots\text{-Nb-O}\dots$ chains. In $\text{BiScO}_3/\text{LaAlO}_3$ and $\text{PbTiO}_3/\text{BiScO}_3$ superlattices, additional out-of-phase, xy -polarized displacements of Bi and oxygen atoms lying in the same xy plane are stronger; this displacement pattern is characteristic of BiScO_3 . A similar displacement pattern is also typical for unstable modes at the Z point in these superlattices. At the Γ point, the described displacement pattern corresponds to a doubly degenerate ferroelectric E mode (Γ_5). [80]

Of two possible polar phases resulting from the condensation of the unstable ferroelectric E mode,

TABLE I. Energies (per 10-atom supercell) of different low-symmetry phases resulting from the condensation of unstable phonons in the high-symmetry $P4mm$ phase of short-period $\text{KNbO}_3/\text{BaTiO}_3$ and $\text{KNbO}_3/\text{SrZrO}_3$ superlattices.

Phase	Unstable phonon	Energy (meV)	Phase	Unstable phonon	Energy (meV)
$\text{KNbO}_3/\text{BaTiO}_3$ superlattice					
$P4mm$	—	0	Pm	$\Gamma_5(\eta, 0)$	-27.8
$Abm2$	R_4	-13.8	$Cmc2_1$	$Z_5(\eta, \eta)$	-31.0
$Pma2$	X_4	-14.8	Cm	$\Gamma_5(\eta, \eta)$	-38.6
$Pmc2_1$	$Z_5(\eta, 0)$	-21.3			
$\text{KNbO}_3/\text{SrZrO}_3$ superlattice					
$P4mm$	—	0	Pc	$Z_5(\eta, 0) + \Gamma_5(0, \xi)$	-19.2
$I4cm$	A_4	-1.3	$Pma2$	$M_5(\eta, 0)$	-19.9
$P4bm$	M_4	-2.1	Cm	$\Gamma_5(\eta, \eta)$	-20.0
$Abm2$	R_4	-4.7	$P2$	$X_3 + X_4$	-20.7
$Pma2$	X_4	-6.7	Cc	$A_4 + \Gamma_5(\eta, \eta)$	-24.1
$Pmm2$	X_3	-12.4	Pm	$X_3 + \Gamma_5(0, \eta)$	-24.9
$Pmc2_1$	$Z_5(\eta, 0)$	-12.9	$Cmm2$	$M_5(\eta, \eta)$	-26.9
Pm	$\Gamma_5(\eta, 0)$	-13.7	Pm	$X_3 + \Gamma_5(\eta, 0)$	-27.6
Pc	$R_4 + \Gamma_5(\eta, 0)$	-15.4	Pm	$M_5(\eta, 0) + \Gamma_5(\xi, \xi)$	-36.9
Cm	$A_4 + \Gamma_5(\eta, 0)$	-16.0	Cm	$M_4 + \Gamma_5(\eta, 0)$	-39.4
Pc	$X_4 + \Gamma_5(\eta, 0)$	-17.0	Cm	$M_5(\eta, \eta) + \Gamma_5(0, \xi)$	-40.2
$Cmc2_1$	$Z_5(\eta, \eta)$	-18.9	Pc	$M_4 + \Gamma_5(\eta, \eta)$	-51.9

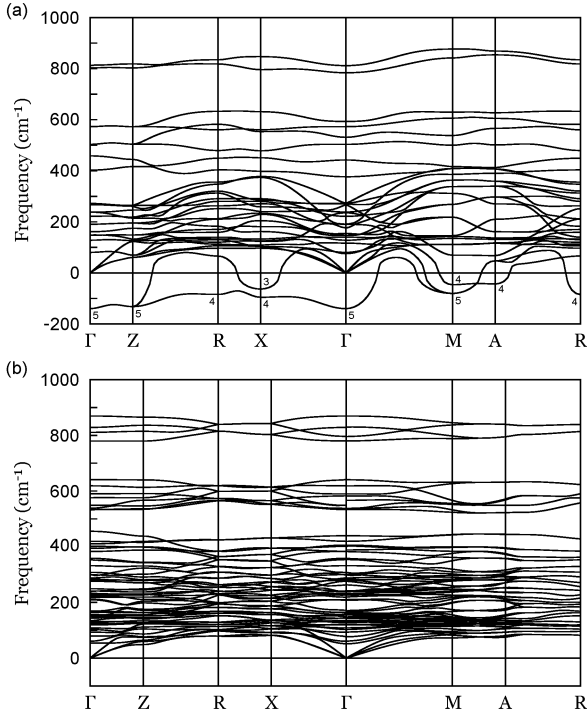


FIG. 4. Phonon spectrum of the $\text{KNbO}_3/\text{SrZrO}_3$ superlattice (a) in the high-symmetry $P4mm$ phase and (b) in the ground-state Pc phase. The numbers near the curves indicate the symmetry of unstable modes.

the Cm phase with atomic displacements along the $[110]$ direction has the lowest energy in all systems except for $\text{KNbO}_3/\text{LaAlO}_3$, $\text{PbTiO}_3/\text{LaGaO}_3$, and $\text{SrTiO}_3/\text{BiScO}_3$. The predominant $[111]$ displacements correlate with the fact that at normal conditions, bulk BaTiO_3 and KNbO_3 are polarized along the $[111]$ direction. The same polarization direction is also characteristic of BiScO_3 when the octahedral rotations are turned off. As an example, the energies of different low-symmetry phases for the $\text{KNbO}_3/\text{BaTiO}_3$ superlattice are given in Table I. It is seen that the structures obtained from the condensation of Z_5 , R_4 , and X_4 unstable phonons have a higher energy as compared to the energy of the Cm phase. The lattice parameters and atomic positions in ground-state structures of this and other superlattices studied in this work are given in Tables S2–S26 of the Supplementary data.

The absence of the ferroelectric instability in the $P4mm$ phase of $\text{PbTiO}_3/\text{KTaO}_3$ and $\text{PbTiO}_3/\text{LaAlO}_3$ SLs can be explained by a tendency of bulk PbTiO_3 to be polarized along the $[001]$ axis. This instability was also absent in $\text{SrTiO}_3/\text{LaAlO}_3$ and $\text{KTaO}_3/\text{LaAlO}_3$ superlattices, in which both constituents are nonpolar. In addition, the ferroelectric instability did not appear in the $\text{BaTiO}_3/\text{LaAlO}_3$ superlattice, in which its absence is a result of the strong (by 2.3%) in-plane compression of the BaTiO_3 layers. Our calculations of the influence of strain on the ground-state structure of BaTiO_3 showed that the biaxial compression of 1% is already sufficient for the $P4mm$ phase to become the most stable polar

phase in this material, in agreement with [81, 82].

Along with the ferroelectric instability, in the high-symmetry $P4mm$ phase of twelve superlattices with the polar discontinuity (except for $\text{KNbO}_3/\text{PbTiO}_3$, $\text{KNbO}_3/\text{BaTiO}_3$, $\text{KNbO}_3/\text{BaZrO}_3$, $\text{BaTiO}_3/\text{KTaO}_3$, and $\text{KTaO}_3/\text{PbTiO}_3$), an antiferrodistortive instability with octahedra rotations around the z axis is observed. This is clearly seen by the appearance of unstable phonons on the M - A line (Fig. 3). The appearance of the AFD instability in a superlattice clearly correlates with its existence in one or both components of the SL (SrTiO_3 , SrZrO_3 , LaAlO_3 , BiScO_3). A comparison of the energies of phases resulting from the condensation of phonons at M and A points of the Brillouin zone shows that of two phases resulting from the M_4 phonon condensation (space group $P4bm$) and from the A_4 phonon condensation (space group $I4cm$), the $P4bm$ phase was energetically more favorable in all cases except for the $\text{PbTiO}_3/\text{BiScO}_3$ superlattice.

The most complex picture is observed in superlattices, in which both the ferroelectric and AFD instabilities are simultaneously present in the $P4mm$ phase. Since the energy difference between the $P4bm$ and $I4cm$ phases is small and both phases can exhibit the ferroelectric instability, it was necessary to consider all polar subgroups of these phases when searching for the ground state. The $\text{KNbO}_3/\text{SrZrO}_3$ superlattice is an example of such a system. Its phonon spectrum is shown in Fig. 4, and the energies of different phases are given in Table I.

The calculations show that the ferroelectric instability of the $P4bm$ and $I4cm$ phases is characteristic of $\text{KNbO}_3/\text{SrTiO}_3$, $\text{KNbO}_3/\text{SrZrO}_3$, $\text{SrTiO}_3/\text{KTaO}_3$ superlattices and all SLs containing BiScO_3 . Of two phases, $Cm(2)$ and Pc , into which the $P4bm$ structure can transform upon the polar distortion, the Pc phase with polarization along the $[110]$ direction of the pseudocubic cell had lower energy in all SLs except for $\text{PbTiO}_3/\text{LaGaO}_3$. Of two phases, Cc and one more phase of the Cm symmetry, $Cm(3)$, into which the $I4cm$ structure can transform upon the polar distortion, the Cc phase whose polarization is also directed along the $[110]$ direction of the pseudocubic cell usually had a lower energy. In $\text{BiScO}_3/\text{LaAlO}_3$ and $\text{KNbO}_3/\text{BiScO}_3$ superlattices, it was the $Cm(3)$ phase which had a lower energy, but this phase has never become the ground state. In $\text{KNbO}_3/\text{SrTiO}_3$ and $\text{SrTiO}_3/\text{KTaO}_3$ superlattices, the energy difference between the Cc and Pc phases was only 0.5–0.7 meV, whereas in other systems it was within 8–80 meV. Since the calculations proved the stability of both Cc and Pc phases in the two superlattices, the Cc phase should be considered as a metastable one. As the energy difference between the two phases is very small, there is a real possibility that both structures can occur in an experiment simultaneously. That is why the properties of these superlattices were calculated below for both phases, Pc and Cc .

The $\text{PbTiO}_3/\text{LaGaO}_3$ superlattice is the only one in which the $Cm(2)$ phase is the ground state. It originates

from the $P4bm$ phase and has the polarization directed along the $[x0z]$ direction of the pseudocubic cell.

In addition to the unstable M_4 mode discussed above, in phonon spectra of the $P4mm$ phase of nine SLs ($\text{KNbO}_3/\text{SrTiO}_3$, $\text{KNbO}_3/\text{SrZrO}_3$, $\text{SrTiO}_3/\text{LaAlO}_3$, $\text{PbTiO}_3/\text{LaAlO}_3$, $\text{PbTiO}_3/\text{LaGaO}_3$, and all SLs containing BiScO_3) one more doubly degenerate unstable M_5 mode is observed (Fig. 4). This mode describes the octahedra rotations around one or both of the x and y axes. The distortions described by this mode with the order parameters of $(\eta, 0)$ and (η, η) result in the $Pma2$ and $Cmm2$ phases whose energies are usually higher than that of the $P4bm$ phase (except for $\text{PbTiO}_3/\text{LaGaO}_3$, $\text{SrTiO}_3/\text{BiScO}_3$, $\text{KNbO}_3/\text{BiScO}_3$, and $\text{KNbO}_3/\text{SrZrO}_3$ SLs). Both the $Pma2$ and $Cmm2$ phases are characterized by the ferroelectric instability. An analysis of the polar subgroups of these phases (with Pc , Cm , and Pm space groups) shows that the Pc phase has the lowest energy among them. It should be noted, however, that in the $\text{BiScO}_3/\text{LaAlO}_3$ and $\text{PbTiO}_3/\text{LaGaO}_3$ superlattices, the structure of this phase differs from that of the Pc phase, which originates from the $P4bm$ phase. In the $\text{BiScO}_3/\text{LaAlO}_3$ superlattice, this new $Pc(2)$ phase becomes the ground-state structure because its energy is lower than that of the Pc phase originating from the $P4bm$ phase. In the $\text{PbTiO}_3/\text{LaGaO}_3$ superlattice, the energy of the $Pc(2)$ phase is intermediate between those of the Pc phase and ground-state $Cm(2)$ structure. As the $Pc(2)$ phase demonstrates its stability with respect to all acoustic and optical distortions, we conclude that this is a metastable phase.

In two latter superlattices, $\text{BiScO}_3/\text{LaAlO}_3$ and $\text{PbTiO}_3/\text{LaGaO}_3$, we encounter a situation when the metastable solutions appear. The cause of this metastability is that the relaxation paths of the $P4bm$ and $Pma2$ ($Cmm2$) phases, in which the rotations are described by the M_4 and M_5 irreducible representations, are separated by a potential barrier. In other superlattices, these barriers are absent, and the structures, regardless of the initial rotation pattern, relax to the same ground-state Pc structure. It may seem strange why the same phase appears as a result of condensation of distortions described by two different irreducible representations. However, it should be taken into account that the vertical axis of the octahedra in the Pc phase is slightly inclined, which means that, in fact, this phase is described by two non-zero rotations around the coordinate axes. This explains why two structures, in which rotational distortions are described by different irreducible representations, relax to the same phase when the polar distortions are turned on.

In $\text{SrTiO}_3/\text{LaAlO}_3$ and $\text{PbTiO}_3/\text{LaAlO}_3$ superlattices, both the $Pma2$ and $Cmm2$ phases relax to the $P4bm$ structure when the polar distortions are turned on. Here, as in the case of the $\text{KNbO}_3/\text{LaAlO}_3$ SL, the strong AFD instability of LaAlO_3 results in a complete suppression of the ferroelectric instability which was present in the high-symmetry $P4mm$ phase.

TABLE II. Calculated polarization and energy gain resulting from the in-plane ferroelectric distortion for all studied short-period superlattices.

Superlattice	Space group	P_x	P_y	P_z	ΔE (meV)
		(C/m ²)			
KNbO ₃ /PbTiO ₃	<i>Cm</i>	0.181	0	0.567	3.3
KNbO ₃ /BaTiO ₃	<i>Cm</i>	0.338	0	-0.033	38.6
KNbO ₃ /BaZrO ₃	<i>Cm</i>	0.229	0	0.181	33.8
KNbO ₃ /SrTiO ₃	<i>Pc</i>	0.281	0	0.066	53.3; 9.0 ^a
KNbO ₃ /SrZrO ₃	<i>Pc</i>	0.268	0	0.187	51.9; 49.8 ^a
BaTiO ₃ /KTaO ₃	<i>Cm</i>	0.180	0	0.130	9.7
BaTiO ₃ /LaAlO ₃	<i>P4bm</i>	0	0	0.057	—
SrTiO ₃ /KTaO ₃	<i>Pc</i>	0.105	0	0.141	11.9; 0.8 ^a
SrTiO ₃ /LaAlO ₃	<i>P4bm</i>	0	0	0.012	—
SrTiO ₃ /BiScO ₃	<i>Pc</i>	0.501	0	0.329	671.1; 331.1 ^a
PbTiO ₃ /KTaO ₃	<i>P4mm</i>	0	0	0.454	—
PbTiO ₃ /LaAlO ₃	<i>P4bm</i>	0	0	0.119	—
PbTiO ₃ /LaGaO ₃	<i>Cm(2)</i>	0.073	0	-0.192	24.0 ^a
PbTiO ₃ /BiScO ₃	<i>Pc</i>	0.710	0	0.330	865.5; 349.3 ^a
KNbO ₃ /LaAlO ₃	<i>P4bm</i>	0	0	0.061	—
KTaO ₃ /LaAlO ₃	<i>P4bm</i>	0	0	0.109	—
KNbO ₃ /BiScO ₃	<i>Pc</i>	0.558	0	0.241	381.3; 281.5 ^a
KNbO ₃ /NaTaO ₃	<i>Pc</i>	0.302	0	0.119	26.5; 26.4 ^a
BaTiO ₃ /SrZrO ₃	<i>Pc</i>	0.234	0	0.072	186.8
BaTiO ₃ /SrSnO ₃	<i>Pc</i>	0.189	0	0.072	275.9
BiScO ₃ /LaAlO ₃	<i>Pc(2)</i>	0.493	0	-0.116	535.1; 189.3 ^a
BaTiO ₃ /SrTiO ₃	<i>Cm</i>	0.233	0	0.061	4.8
KNbO ₃ /KTaO ₃	<i>Cm</i>	0.223	0	0.119	11.7
PbTiO ₃ /PbZrO ₃	<i>Pc</i>	0.586	0	0.314	488.2; 147.4 ^a
KNbO ₃ /NaNbO ₃	<i>Pmc2₁</i>	0.502	0	0	104.5; 98.6 ^b

^a As compared to the non-polar *P4bm* phase.

^b As compared to the non-polar *P4/mbm* phase.

In all BiScO₃-containing superlattices with the polar discontinuity, one more unstable mode, A_5 , appears in the phonon spectrum at the A point. An analysis of chains of phases induced by the corresponding distortions showed that all obtained phases have the energy much higher than that of the ground-state structure.

The space groups of the energetically most favorable phases obtained for all studied superlattices are given in Table II. It is seen that in superlattices exhibiting only the ferroelectric instability in the high-symmetry *P4mm* phase, the *Cm* phase is the ground state. In superlattices exhibiting only the AFD instability, the *P4bm* phase is the ground state. And, finally, in superlattices in which both instabilities are present, the *Pc* phase is the ground state, with the exception of the KNbO₃/LaAlO₃ and PbTiO₃/LaGaO₃ superlattices. In the first of these exceptions, the AFD instability suppresses the ferroelectric one, and the *P4bm* phase becomes the ground state. In the second of them,

the ground-state structure is *Cm(2)*. The discrepancy between our results and those obtained for the KNbO₃/BaTiO₃ SL in [67] stems from the fact that the calculations in Ref. [67] were performed for the superlattice clamped on the SrTiO₃ substrate; at these boundary conditions, the *P4mm* phase is indeed the ground state.

Table II also presents the energy gain ΔE per 10-atom formula unit, which results from the in-plane ferroelectric distortion. The obtained values show that, at room temperature, the predicted ground-state structures are likely to be observed in the KNbO₃/BaTiO₃, KNbO₃/BaZrO₃, KNbO₃/SrZrO₃, SrTiO₃/BiScO₃, PbTiO₃/BiScO₃, and KNbO₃/BiScO₃ superlattices. For the ground-state structures of all superlattices, the calculated spontaneous polarization and components of the piezoelectric tensor are presented in the following sections.

2. Calculation of polarization

Classical electrostatics of an electrically neutral interface between two dielectrics requires that the electric displacement field components normal to this interface are equal in two materials. If the materials are ferroelectrics and have different spontaneous polarizations, a bound electric charge appears at the interface, and the electric field generated by it makes the electric displacement fields equal in two materials.

In superlattices with the polar discontinuity, a violation of the order of charged AO and BO_2 planes generates an additional electrostatic perturbation at the interfaces and creates a polarization jump of $\Delta P = e/2a^2$ in superlattices with a change in ionic charges of components by e and $\Delta P = e/a^2$ in superlattices with a change in the ionic charges by $2e$ (here a is the in-plane lattice parameter of the superlattice) [60]. An elegant solution to this problem within the modern theory of polarization, which is valid in the general case, was proposed in [64]. An application of this approach to our superlattices enables us to calculate the electric displacement field in them and to use it to determine the *average* polarization in the SLs. In this work, we are interested precisely in this property. The polarization values in individual layers of a SL can be calculated by correcting the obtained average polarization taking into account the jump in the ionic contribution to the Berry phase at the interface and dielectric constants of individual components.[83]

When calculating the polarization by the Berry phase method, it should be borne in mind that the ionic contributions to the Berry phase are different in nonpolar $Pm\bar{3}m$ phases of I-V, II-IV, and III-III perovskites [84]. That is why for each SL with the polar discontinuity it is necessary first to find the Berry phase for the nonpolar structure before calculating the polarization. Unfortunately, in our case, the calculation of the z component of the Berry phase becomes a problem because it is impossible to reverse the polarization or construct a non-polar structure for the high-symmetry *P4mm* phase, which

does not have σ_z mirror plane. To estimate P_z , we considered unrelaxed structures with ideal atomic positions corresponding to the cubic perovskite structure in both layers. In this structure, the electron contribution to the Berry phase is nonzero because of the redistribution of the electron density between the layers, and the ionic contribution reflects the difference in the Berry phases of individual perovskites. The average polarization in a superlattice was calculated using standard formulas from a change in the Berry phase upon the transition from the above-described unrelaxed structure to the ground-state one. To correctly determine the polarization from the change in the Berry phase, which is well-defined modulo 2π , for all superlattices the calculations were also performed for at least one intermediate point at which the atoms are halfway between the ground-state and unrelaxed structures.

The calculated polarizations are given in Table II. The components of the polarization vector are given relative to the axes of the standard crystallographic settings for tetragonal and monoclinic unit cells (their axes are often rotated in the xy plane relative to each other by 45°). A comparison of polarizations calculated for structures with and without octahedral rotations shows that in SLs with the Pc ground-state structure, the neglect of these rotations can result in an error in determining P_z up to 30% and, in some cases, even in an error in the sign of this quantity. For the $P4mm$ phase, our values reasonably agree with the published values of $P_z = 0.532$ C/m² for PbTiO₃/KNbO₃ [72], $P_z = 0.202$ C/m² for PbTiO₃/LaAlO₃ [72], and $P_z = 0.38$ C/m² for PbTiO₃/KTaO₃ [85] SLs.

3. Piezoelectric properties

The reason for our interest to ferroelectric instability in superlattices with the polar discontinuity is that in such SLs it is possible to obtain rather high piezoelectric coefficients resulting from the in-plane ferroelectric phase transitions appearing in them. The literature data on the piezoelectric properties of such superlattices are limited to calculations for the high-symmetry $P4mm$ phase of PbTiO₃/LaAlO₃ and KNbO₃/PbTiO₃ SLs [71, 72] and of the PbTiO₃/KTaO₃ one [85]. As the ground-state structure of the first two superlattices differs from $P4mm$, more correct calculations for these SLs are needed. For other superlattices considered in this work, data on their piezoelectric properties are absent.

In superlattices with a tetragonal ground-state structure, in which the polarization is directed along the z axis, five components of the piezoelectric tensor $d_{i\nu}$ are nonzero. Among them, the highest values of $d_{i\nu}$ are obtained for PbTiO₃/KTaO₃ and PbTiO₃/LaAlO₃ SLs (Table III). Interestingly, among these coefficients, the d_{15} values turned out to be the largest. This coefficient characterizes the polarization P_x that appears as a result of the xz shear strain of the unit cell, that is,

as a result of the inclination of the polarization vector. However, no clear correlation between d_{15} and P_z was observed in tetragonal SLs. Moreover, in the related system, BaTiO₃/LaAlO₃, the piezoelectric coefficients were unexpectedly low (Table III). This means that the inclination of the polarization vector is not an effective way for obtaining high piezoelectric coefficients.

In superlattices with a monoclinic ground-state structure, in which the polarization vector lies in the xz plane, the piezoelectric tensor is characterized by ten nonzero components. In these SLs, the highest values of $d_{i\nu}$ are the d_{24} and d_{26} coefficients, which describe the appearance of polarization in the y direction normal to the xz plane under the yz and xy shear strain. An analysis of the obtained data also does not find a clear correlation between the piezoelectric coefficients and the average polarization. Stretching the unit cells of these superlattices in the xz plane changes the polarization, but the corresponding piezoelectric coefficients (d_{11} and d_{33} in Table III) are not the largest.

To understand the mechanism of the appearance of high piezoelectric coefficients in some superlattices with the polar discontinuity, we analyzed the third-rank tensors $\partial u_\alpha^i / \partial \sigma_{\mu\nu}$. This tensor characterizes the displacement of the i th atom in the unit cell in the α direction produced by strain $\sigma_{\mu\nu}$. It turned out that in SLs exhibiting strong piezoelectricity, the values of some components of these tensors for some atoms reach 10–15 Å (that is, the unit cell strain of 1% generates atomic displacements exceeding 0.1 Å). For example, in the PbTiO₃/LaAlO₃ superlattice, such atoms are Pb(1), La(6), and two oxygen atoms O(4) and O(14) located in the TiO₂ layer (Table IV); the contributions of O(8) and O(9) oxygen atoms located in the AlO₂ layer are 25 times smaller.

The fact that strong distortions in the PbTiO₃/LaAlO₃ SL are observed in the TiO₂ layer suggests that the Ti(2) atom also actively participates in the appearance of polarization. Indeed, the displacement pattern of the Pb, Ti, and O atoms in the PbO and TiO₂ layers resembles that of the polar mode in PbTiO₃. A more detailed analysis of atomic displacements in monoclinically strained SL, whose deformation is described by a nonzero component $\sigma_{xz} = 0.005$, simultaneously finds two types of distortions: the rotations of corner-linked TiO₆ and AlO₆ octahedra around the x axis, resembling rotations described by an unstable phonon at the R point of the cubic perovskite structure, and out-of-phase (polar) displacements of Pb(1), La(6), Ti(2), O(4), and O(14) atoms along the x axis, like in the polar mode in PbTiO₃. The observed displacement pattern is very close (with the correlation coefficient of 0.902) to the eigenvector of the soft E mode with a surprisingly low frequency of 27 cm⁻¹ in the phonon spectrum of the $P4bm$ phase of this SL. Under the influence of strain, the irreducible representation E reduces to a sum of $A' + A''$ irreducible representations of the low-symmetry Cm phase, and the structure distorts according to the eigenvector of the full-symmetry A' mode. In other SLs

TABLE III. Nonzero components of the piezoelectric tensor $d_{i\nu}$ (in pC/N) for the ground-state structures of all studied short-period superlattices.

Superlattice	d_{11}	d_{12}	d_{13}	d_{15}	d_{24}	d_{26}	d_{31}	d_{32}	d_{33}	d_{35}
KNbO ₃ /PbTiO ₃	13.4	3.7	-13.9	158.3	273.3	137.3	-3.0	-2.9	-10.9	-0.8
KNbO ₃ /BaTiO ₃	23.5	9.6	-12.7	3.8	-2.8	106.4	10.7	7.9	-16.3	17.4
KNbO ₃ /BaZrO ₃	16.3	4.7	-11.7	5.6	7.9	20.8	-8.9	-7.3	16.7	1.8
KNbO ₃ /SrTiO ₃	35.9	15.3	-19.1	8.3	41.7	151.0	-22.0	-12.1	16.1	9.4
KNbO ₃ /SrZrO ₃	30.8	10.1	-18.8	9.1	11.0	85.5	-18.1	-9.8	17.7	12.9
BaTiO ₃ /KTaO ₃	19.2	9.5	-18.5	2.5	7.9	25.3	-18.1	-11.6	43.4	10.1
BaTiO ₃ /LaAlO ₃	—	—	—	1.4	1.4	—	3.0	3.0	-4.6	—
SrTiO ₃ /KTaO ₃	39.7	22.8	-27.6	28.2	46.9	41.2	-18.4	-13.0	26.1	-4.2
SrTiO ₃ /LaAlO ₃	—	—	—	2.0	2.0	—	1.0	1.0	-1.6	—
SrTiO ₃ /BiScO ₃	23.6	5.4	-6.0	14.3	17.9	24.6	-4.7	0.6	11.8	12.2
PbTiO ₃ /KTaO ₃	—	—	—	91.4	91.4	—	-8.8	-8.8	41.2	—
PbTiO ₃ /LaAlO ₃	—	—	—	158.6	158.6	—	-4.3	-4.3	-2.8	—
PbTiO ₃ /LaGaO ₃	19.1	-5.8	-3.0	-29.6	15.1	-35.1	7.8	-2.9	-18.5	4.3
PbTiO ₃ /BiScO ₃	31.1	2.7	-7.4	5.1	1.5	47.0	-2.3	-4.0	18.5	13.6
KNbO ₃ /LaAlO ₃	—	—	—	5.7	5.7	—	1.1	1.1	-0.8	—
KTaO ₃ /LaAlO ₃	—	—	—	5.3	5.3	—	-0.8	-0.8	3.7	—
KNbO ₃ /BiScO ₃	19.2	9.2	-5.9	10.0	23.2	51.2	-0.5	3.9	2.1	6.9
KNbO ₃ /NaTaO ₃	90.2	19.8	-97.1	24.3	-16.0	70.2	154.6	43.1	-209.2	73.5
BaTiO ₃ /SrZrO ₃	23.3	4.9	-12.8	1.2	2.6	19.3	3.9	4.0	-7.8	5.1
BaTiO ₃ /SrSnO ₃	23.9	6.6	-12.7	-7.1	-6.4	23.2	-1.0	-2.2	3.2	2.1
BiScO ₃ /LaAlO ₃	30.2	-1.1	-5.9	-5.7	8.3	23.1	0.3	1.3	-3.5	10.5
BaTiO ₃ /SrTiO ₃	103.5	37.4	-117.1	-59.5	21.1	187.9	-287.3	-131.5	460.5	288.1
KNbO ₃ /KTaO ₃	108.3	60.4	-157.1	-15.9	18.7	123.9	-181.6	-111.3	315.5	45.4
PbTiO ₃ /PbZrO ₃	62.1	12.5	-38.8	3.2	29.9	132.7	-45.8	-19.5	70.4	26.6
KNbO ₃ /NaNbO ₃	17.9	5.3	-9.2	—	—	153.0	—	—	—	60.1

with lower piezoelectric properties, the frequencies of the corresponding modes were higher (40–120 cm⁻¹), but we didn't find simple correlations between the frequencies and effective charges of these modes and the piezoelectric properties. This question needs more detailed investigation.

A comparison of the piezoelectric properties of the metastable Cc phase and the ground-state Pc phase in KNbO₃/SrTiO₃ and SrTiO₃/KTaO₃ superlattices, in which the energy difference between the two structures is very small, shows that their piezoelectric tensors are quite close to each other (Table V). This means that a change in the character of the octahedra rotations weakly affects the piezoelectric properties of SLs.

According to our calculations, the piezoelectric coefficients in studied superlattices can reach 150–270 pC/N. A comparison of the obtained results with the published data in some cases finds their good agreement. For example, for the $P4mm$ phase of PbTiO₃/LaAlO₃ SL our result $e_{33} = -3.52$ C/m² is quite close to the value $e_{33} = -2.85$ C/m² obtained in [71]. However, our value of $d_{33} = -18.9$ pC/N for the same phase of the same SL differs from the value $d_{33} = 13.9$ pC/N obtained in [72]:

these values are close in magnitude, but have a different sign. An additional reason for the stronger discrepancies here may be a neglect of the difference in the displacements and effective charges of the O atoms in Ref. [72] (according to our data, the effective charges varies from -2.07 to -5.84). As for the PbTiO₃/KTaO₃ SL studied in [85], the e_{33} and e_{15} piezoelectric coefficients obtained there are almost 100 times less than our data, and the e_{31} value is close to our result in magnitude, but differs in sign.

In conclusion, it was interesting to compare the piezoelectric properties of superlattices with the polar discontinuity with those of “isoelectronic” superlattices: (1) SLs without the polar discontinuity, in which the broken symmetry and high-symmetry $P4mm$ structure are formed, by analogy with [25], as a result of the absence of the mirror symmetry in the sequence of layers (BaTiO₃/SrZrO₃, BaTiO₃/SrSnO₃, KNbO₃/NaTaO₃, and BiScO₃/LaAlO₃), and (2) ordinary SLs with one substituted atom (BaTiO₃/SrTiO₃, KNbO₃/KTaO₃, and two famous systems known for their high piezoelectric properties, PbTiO₃/PbZrO₃ and “lead-free” KNbO₃/NaNbO₃). The piezoelectric prop-

TABLE IV. The values of the $\partial u_1^i / \partial \sigma_{15}$ component of the $\partial u_\alpha^i / \partial \sigma_{\mu\nu}$ tensor (in Å) for all atoms in the ground-state structure of $\text{PbTiO}_3/\text{LaAlO}_3$ and $\text{BaTiO}_3/\text{LaAlO}_3$ superlattices ($P4bm$ phase) and in ordinary superlattices, $\text{PbTiO}_3/\text{PbZrO}_3$ (Pc phase) and $\text{KNbO}_3/\text{NaNbO}_3$ ($Pmc2_1$ phase), of systems known for their piezoelectric properties. Atoms 1–10 are numbered according to Fig. 1; atoms 11–20 are located in the second part of the doubled unit cell of the high-temperature phase and are shifted from atoms 1–10 along the x axis. For atomic positions of all atoms see tables in the Supplementary data.

Atom i	$\text{PbTiO}_3/\text{LaAlO}_3$	$\text{BaTiO}_3/\text{LaAlO}_3$	$\text{PbTiO}_3/\text{PbZrO}_3$	$\text{KNbO}_3/\text{NaNbO}_3$
1	+5.18	+0.09	+0.35	+0.00
2	+2.37	-0.08	+0.03	-0.58
3	-1.19	+0.24	+0.14	-0.31
4	-5.61	+0.10	+0.17	-0.51
5	-1.02	-0.11	+0.49	+0.00
6	+4.56	+0.73	+0.44	+0.00
7	+0.76	+0.02	-0.23	+0.58
8	-0.21	-0.31	-0.31	+0.31
9	-0.22	-0.15	-0.83	+0.51
10	-0.84	-0.10	-0.42	+0.00
11	+1.71	-0.38	+0.01	+0.00
12	+2.37	-0.08	+0.08	-0.41
13	-1.19	+0.24	-0.11	-0.51
14	-5.61	+0.10	-0.43	-1.15
15	-1.02	-0.11	+0.47	+0.00
16	+0.48	+0.37	+0.76	+0.00
17	+0.76	+0.02	-0.19	+0.41
18	-0.21	-0.31	-0.06	+0.51
19	-0.22	-0.15	-0.26	+1.15
20	-0.84	-0.10	-0.12	+0.00

TABLE V. Nonzero components of the piezoelectric tensor $d_{i\nu}$ (in pC/N) in the ground and metastable states of two short-period superlattices with the polar discontinuity.

Phase	d_{11}	d_{12}	d_{13}	d_{15}	d_{24}	d_{26}	d_{31}	d_{32}	d_{33}	d_{35}
KNbO ₃ /SrTiO ₃ superlattice										
<i>Pc</i>	35.9	15.3	-19.1	8.3	41.7	151.0	-22.0	-12.1	16.1	9.4
<i>Cc</i>	35.0	14.8	-18.3	7.7	41.4	154.0	-21.4	-11.6	15.7	11.1
SrTiO ₃ /KTaO ₃ superlattice										
<i>Pc</i>	39.7	22.8	-27.6	28.2	46.9	41.2	-18.4	-13.0	26.1	-4.2
<i>Cc</i>	39.2	22.3	-27.4	27.1	45.7	41.1	-18.6	-13.1	26.3	-3.7

erties of these superlattices are given in the last eight lines of Table III. It is seen that in spite of a large scatter of the data, superlattices with the polar discontinuity are not much different in their piezoelectric properties from other superlattices (high piezoelectric properties of $\text{BaTiO}_3/\text{SrTiO}_3$ and $\text{KNbO}_3/\text{KTaO}_3$ SLs, as follows from the corresponding values of ΔE (Table II), can be realized only at low temperatures). Thus, the only advantage of superlattices with the polar discontinuity as well as of SLs with broken symmetry is that one component of polarization in them is not switchable.

IV. CONCLUSIONS

First-principles calculations have been used to study the stability of a high-symmetry $P4mm$ polar phase in seventeen ferroelectric perovskite superlattices with the polar discontinuity. In most superlattices, this phase exhibits either the ferroelectric instability or the antiferrodistortive one, or both of them simultaneously. For each superlattice, the ground-state structure, the structure of possible metastable phases, spontaneous polarization, and piezoelectric properties were calculated. A comparison of the piezoelectric properties of superlattices with the polar discontinuity and those without the polar discontinuity (superlattices with broken symmetry

and ordinary superlattices) showed that these properties are not much different. It was demonstrated that high piezoelectric coefficients (up to 150–270 pC/N) in some superlattices with the polar discontinuity are due to the appearance of strong lattice distortions, whose symmetry follows that of a low-lying polar phonon mode of the ground-state structure under the influence of external strain.

Data availability statement

All data included in this study are available upon request from the author.

Declaration of competing interests

The author declares that he has no known competing financial interests or personal relationships that could

have appeared to influence the work reported in this paper.

ACKNOWLEDGMENTS

This work was partially supported by the Russian Foundation for Basic Research under Grant 17-02-01068.

Appendix A: Supplementary data

Supplementary data associated with this article can be found in the online version at <https://doi.org/10.1016/j.commat.2020.110113>.

-
- [1] K. Iijima, T. Terashima, Y. Bando, K. Kamigaki, and H. Terauchi, Atomic layer growth of oxide thin films with perovskite-type structure by reactive evaporation, *J. Appl. Phys.* **72**, 2840 (1992).
- [2] T. Tsurumi, T. Suzuki, M. Yamane, and M. Daimon, Fabrication of barium titanate/strontium titanate artificial superlattice by atomic layer epitaxy, *Jap. J. Appl. Phys.* **33**, 5192 (1994).
- [3] H. Tabata, H. Tanaka, and T. Kawai, Formation of artificial BaTiO₃/SrTiO₃ superlattices using pulsed laser deposition and their dielectric properties, *Appl. Phys. Lett.* **65**, 1970 (1994).
- [4] H. Tabata and T. Kawai, Dielectric properties of strained (Sr,Ca)TiO₃/(Ba,Sr)TiO₃ artificial lattices, *Appl. Phys. Lett.* **70**, 321 (1997).
- [5] B. D. Qu, M. Evstigneev, D. J. Johnson, and R. H. Prince, Dielectric properties of BaTiO₃/SrTiO₃ multilayered thin films prepared by pulsed laser deposition, *Appl. Phys. Lett.* **72**, 1394 (1998).
- [6] E. D. Specht, H.-M. Christen, D. P. Norton, and L. A. Boatner, X-ray diffraction measurement of the effect of layer thickness on the ferroelectric transition in epitaxial KTaO₃/KNbO₃ multilayers, *Phys. Rev. Lett.* **80**, 4317 (1998).
- [7] D. O'Neill, R. M. Bowman, and J. M. Gregg, Dielectric enhancement and Maxwell–Wagner effects in ferroelectric superlattice structures, *Appl. Phys. Lett.* **77**, 1520 (2000).
- [8] O. Nakagawara, T. Shimuta, T. Makino, S. Arai, H. Tabata, and T. Kawai, Epitaxial growth and dielectric properties of (111) oriented BaTiO₃/SrTiO₃ superlattices by pulsed-laser deposition, *Appl. Phys. Lett.* **77**, 3257 (2000).
- [9] T. Shimuta, O. Nakagawara, T. Makino, S. Arai, H. Tabata, and T. Kawai, Enhancement of remanent polarization in epitaxial BaTiO₃/SrTiO₃ superlattices with “asymmetric” structure, *J. Appl. Phys.* **91**, 2290 (2002).
- [10] J. Sigman, D. P. Norton, H. M. Christen, P. H. Fleming, and L. A. Boatner, Antiferroelectric behavior in symmetric KNbO₃/KTaO₃ superlattices, *Phys. Rev. Lett.* **88**, 097601 (2002).
- [11] J. Kim, Y. Kim, Y. S. Kim, J. Lee, L. Kim, and D. Jung, Large nonlinear dielectric properties of artificial BaTiO₃/SrTiO₃ superlattices, *Appl. Phys. Lett.* **80**, 3581 (2002).
- [12] L. Kim, D. Jung, J. Kim, Y. S. Kim, and J. Lee, Strain manipulation in BaTiO₃/SrTiO₃ artificial lattice toward high dielectric constant and its nonlinearity, *Appl. Phys. Lett.* **82**, 2118 (2003).
- [13] A. Q. Jiang, J. F. Scott, H. Lu, and Z. Chen, Phase transitions and polarizations in epitaxial BaTiO₃/SrTiO₃ superlattices studied by second-harmonic generation, *J. Appl. Phys.* **93**, 1180 (2003).
- [14] M. Dawber, C. Lichtensteiger, M. Cantoni, M. Veithen, P. Ghosez, K. Johnston, K. M. Rabe, and J.-M. Triscone, Unusual behavior of the ferroelectric polarization in PbTiO₃/SrTiO₃ superlattices, *Phys. Rev. Lett.* **95**, 177601 (2005).
- [15] W. Tian, J. C. Jiang, X. Q. Pan, J. H. Haeni, Y. L. Li, L. Q. Chen, D. G. Schlom, J. B. Neaton, K. M. Rabe, and Q. X. Jia, Structural evidence for enhanced polarization in a commensurate short-period BaTiO₃/SrTiO₃ superlattice, *Appl. Phys. Lett.* **89**, 092905 (2006).
- [16] D. A. Tenne, A. Bruchhausen, N. D. Lanzillotti-Kimura, A. Fainstein, R. S. Katiyar, A. Cantarero, A. Soukiasian, V. Vaithyanathan, J. H. Haeni, W. Tian, D. G. Schlom, K. J. Choi, D. M. Kim, C. B. Eom, H. P. Sun, X. Q. Pan, Y. L. Li, L. Q. Chen, Q. X. Jia, S. M. Nakhmanson, K. M. Rabe, and X. X. Xi, Probing nanoscale ferroelectricity by ultraviolet Raman spectroscopy, *Science* **313**, 1614 (2006).
- [17] M. Dawber, N. Stucki, C. Lichtensteiger, S. Gariglio, P. Ghosez, and J.-M. Triscone, Tailoring the properties of artificially layered ferroelectric superlattices, *Adv. Mater.* **19**, 4153 (2007).
- [18] P. Zubko, N. Stucki, C. Lichtensteiger, and J.-M. Triscone, X-ray diffraction studies of 180° ferroelectric domains in PbTiO₃/SrTiO₃ superlattices under an applied electric field, *Phys. Rev. Lett.* **104**, 187601 (2010).

- [19] Y. I. Yuzyuk, Raman scattering spectra of ceramics, films, and superlattices of ferroelectric perovskites: A review, *Phys. Solid State* **54**, 1026 (2012).
- [20] J. Sinsheimer, S. J. Callori, B. Bein, Y. Benkara, J. Daley, J. Coraor, D. Su, P. W. Stephens, and M. Dawber, Engineering polarization rotation in a ferroelectric superlattice, *Phys. Rev. Lett.* **109**, 167601 (2012).
- [21] Y. A. Tikhonov, A. G. Razumnaya, O. A. Maslova, I. N. Zakharchenko, Y. I. Yuzyuk, N. Ortega, A. Kumar, and R. S. Katiyar, Phase transitions in two- and three-component perovskite superlattices, *Phys. Solid State* **57**, 486 (2015).
- [22] S. Das, Y. L. Tang, Z. Hong, M. A. P. Gonçalves, M. R. McCarter, C. Klewe, K. X. Nguyen, F. Gómez-Ortiz, P. Shafer, E. Arenholz, V. A. Stoica, S.-L. Hsu, B. Wang, C. Ophus, J. F. Liu, C. T. Nelson, S. Saremi, B. Prasad, A. B. Mei, D. G. Schlom, J. Íñiguez, P. García-Fernández, D. A. Muller, L. Q. Chen, J. Junquera, L. W. Martin, and R. Ramesh, Observation of room-temperature polar skyrmions, *Nature* **568**, 368 (2019).
- [23] A. S. Sidorkin, L. P. Nesterenko, Y. Gagou, P. Saint-Gregoire, E. V. Vorotnikov, A. Y. Pakhomov, and N. G. Popravko, Repolarization of ferroelectric superlattices $\text{BaZrO}_3/\text{BaTiO}_3$, *Sci. Rep.* **9**, 18948 (2019).
- [24] G. Sághi-Szabó, R. E. Cohen, and H. Krakauer, First-principles study of piezoelectricity in tetragonal PbTiO_3 and $\text{PbZr}_{1/2}\text{Ti}_{1/2}\text{O}_3$, *Phys. Rev. B* **59**, 12771 (1999).
- [25] N. Sai, B. Meyer, and D. Vanderbilt, Compositional inversion symmetry breaking in ferroelectric perovskites, *Phys. Rev. Lett.* **84**, 5636 (2000).
- [26] J. B. Neaton and K. M. Rabe, Theory of polarization enhancement in epitaxial $\text{BaTiO}_3/\text{SrTiO}_3$ superlattices, *Appl. Phys. Lett.* **82**, 1586 (2003).
- [27] C. Bungaro and K. M. Rabe, Epitaxially strained $[001]$ - $(\text{PbTiO}_3)_1(\text{PbZrO}_3)_1$ superlattice and PbTiO_3 from first principles, *Phys. Rev. B* **69**, 184101 (2004).
- [28] H. N. Lee, H. M. Christen, M. F. Chisholm, C. M. Rouleau, and D. H. Lowndes, Strong polarization enhancement in asymmetric three-component ferroelectric superlattices, *Nature* **433**, 395 (2005).
- [29] K. Johnston, X. Huang, J. B. Neaton, and K. M. Rabe, First-principles study of symmetry lowering and polarization in $\text{BaTiO}_3/\text{SrTiO}_3$ superlattices with in-plane expansion, *Phys. Rev. B* **71**, 100103 (2005).
- [30] L. Kim, J. Kim, D. Jung, J. Lee, and U. V. Waghmare, Polarization of strained $\text{BaTiO}_3/\text{SrTiO}_3$ artificial superlattice: First-principles study, *Appl. Phys. Lett.* **87**, 052903 (2005).
- [31] S. M. Nakhmanson, K. M. Rabe, and D. Vanderbilt, Polarization enhancement in two- and three-component ferroelectric superlattices, *Appl. Phys. Lett.* **87**, 102906 (2005).
- [32] P. Ghosez and J. Junquera, First-principle modeling of ferroelectric oxide nanostructures, in *Handbook of Theoretical and Computational Nanotechnology*, Vol. 9, edited by M. Rieth and W. Schommers (American Scientific Publishers, 2006) pp. 623–728.
- [33] S. Lisenkov and L. Bellaiche, Phase diagrams of $\text{BaTiO}_3/\text{SrTiO}_3$ superlattices from first principles, *Phys. Rev. B* **76**, 020102 (2007).
- [34] Y. L. Li, S. Y. Hu, D. Tenne, A. Soukiassian, D. G. Schlom, X. X. Xi, K. J. Choi, C. B. Eom, A. Saxena, T. Lookman, Q. X. Jia, and L. Q. Chen, Prediction of ferroelectricity in $\text{BaTiO}_3/\text{SrTiO}_3$ superlattices with domains, *Appl. Phys. Lett.* **91**, 112914 (2007).
- [35] E. Bousquet, M. Dawber, N. Stucki, C. Lichtensteiger, P. Hermet, S. Gariglio, J.-M. Triscone, and P. Ghosez, Improper ferroelectricity in perovskite oxide artificial superlattices, *Nature* **452**, 732 (2008).
- [36] X. Wu, M. Stengel, K. M. Rabe, and D. Vanderbilt, Predicting polarization and nonlinear dielectric response of arbitrary perovskite superlattice sequences, *Phys. Rev. Lett.* **101**, 087601 (2008).
- [37] S. Lisenkov, I. Ponomareva, and L. Bellaiche, Unusual static and dynamical characteristics of domain evolution in ferroelectric superlattices, *Phys. Rev. B* **79**, 024101 (2009).
- [38] A. I. Lebedev, Ab initio studies of dielectric, piezoelectric, and elastic properties of $\text{BaTiO}_3/\text{SrTiO}_3$ ferroelectric superlattices, *Phys. Solid State* **51**, 2324 (2009).
- [39] A. I. Lebedev, Ground state and properties of ferroelectric superlattices based on crystals of the perovskite family, *Phys. Solid State* **52**, 1448 (2010).
- [40] X. Wu, K. M. Rabe, and D. Vanderbilt, Interfacial enhancement of ferroelectricity in $\text{CaTiO}_3/\text{BaTiO}_3$ superlattices, *Phys. Rev. B* **83**, 020104 (2011).
- [41] P. Aguado-Puente, P. García-Fernández, and J. Junquera, Interplay of couplings between antiferrodistortive, ferroelectric, and strain degrees of freedom in monodomain $\text{PbTiO}_3/\text{SrTiO}_3$ superlattices, *Phys. Rev. Lett.* **107**, 217601 (2011).
- [42] A. I. Lebedev, Ground-state structure of $\text{KNbO}_3/\text{KTaO}_3$ superlattices: Array of nearly independent ferroelectrically ordered planes, *Phys. Status Solidi B* **249**, 789 (2012).
- [43] P. Aguado-Puente and J. Junquera, Structural and energetic properties of domains in $\text{PbTiO}_3/\text{SrTiO}_3$ superlattices from first principles, *Phys. Rev. B* **85**, 184105 (2012).
- [44] A. I. Lebedev, Properties of $\text{BaTiO}_3/\text{BaZrO}_3$ ferroelectric superlattices with competing instabilities, *Phys. Solid State* **55**, 1198 (2013).
- [45] X. Z. Lu, X. G. Gong, and H. J. Xiang, Polarization enhancement in perovskite superlattices by oxygen octahedral tilts, *Comput. Mater. Sci.* **91**, 310 (2014).
- [46] P. Zubko, J. C. Wojdeł, M. Hadjimichael, S. Fernandez-Pena, A. Sené, I. Luk'yanchuk, J.-M. Triscone, and J. Íñiguez, Negative capacitance in multidomain ferroelectric superlattices, *Nature* **534**, 524 (2016).
- [47] Z. Hong, A. R. Damodaran, F. Xue, S.-L. Hsu, J. Britson, A. K. Yadav, C. T. Nelson, J.-J. Wang, J. F. Scott, L. W. Martin, R. Ramesh, and L.-Q. Chen, Stability of polar vortex lattice in ferroelectric superlattices, *Nano Lett.* **17**, 2246 (2017).
- [48] Z. Hong and L.-Q. Chen, Blowing polar skyrmion bubbles in oxide superlattices, *Acta Mater.* **152**, 155 (2018).
- [49] A. Ohtomo and H. Y. Hwang, A high-mobility electron gas at the $\text{LaAlO}_3/\text{SrTiO}_3$ heterointerface, *Nature* **427**, 423 (2004).
- [50] A. Brinkman, M. Huijben, M. van Zalk, J. Huijben, U. Zeitler, J. C. Maan, W. G. van der Wiel, G. Rijnders, D. H. A. Blank, and H. Hilgenkamp, Magnetic effects at the interface between non-magnetic oxides, *Nature Mater.* **6**, 493 (2007).
- [51] N. Reyren, S. Thiel, A. D. Caviglia, L. F. Kourkoutis, G. Hammerl, C. Richter, C. W. Schneider, T. Kopp, A.-S. Rüetschi, D. Jaccard, M. Gabay, D. A. Muller, J.-M. Triscone, and J. Mannhart, Superconducting interfaces

- between insulating oxides, *Science* **317**, 1196 (2007).
- [52] A. D. Caviglia, S. Gariglio, N. Reyren, D. Jaccard, T. Schneider, M. Gabay, S. Thiel, G. Hammerl, J. Mannhart, and J.-M. Triscone, Electric field control of the $\text{LaAlO}_3/\text{SrTiO}_3$ interface ground state, *Nature* **456**, 624 (2008).
- [53] K. Yang, S. Nazir, M. Behtash, and J. Cheng, High-throughput design of two-dimensional electron gas systems based on polar/nonpolar perovskite oxide heterostructures, *Sci. Rep.* **6**, 34667 (2016).
- [54] B. Yin, P. Aguado-Puente, S. Qu, and E. Artacho, Two-dimensional electron gas at the $\text{PbTiO}_3/\text{SrTiO}_3$ interface: An ab initio study, *Phys. Rev. B* **92**, 115406 (2015).
- [55] J. Ruan, X. Qiu, Z. Yuan, D. Ji, P. Wang, A. Li, and D. Wu, Improved memory functions in multiferroic tunnel junctions with a dielectric/ferroelectric composite barrier, *Appl. Phys. Lett.* **107**, 232902 (2015).
- [56] Q. Wu, L. Shen, M. Yang, J. Zhou, J. Chen, and Y. P. Feng, Giant tunneling electroresistance induced by ferroelectrically switchable two-dimensional electron gas at nonpolar $\text{BaTiO}_3/\text{SrTiO}_3$ interface, *Phys. Rev. B* **94**, 155420 (2016).
- [57] E. Y. Tsymlal and H. Kohlstedt, Tunneling across a ferroelectric, *Science* **313**, 181 (2006).
- [58] J. P. Velev, C.-G. Duan, J. D. Burton, A. Smogunov, M. K. Niranjan, E. Tosatti, S. S. Jaswal, and E. Y. Tsymlal, Magnetic tunnel junctions with ferroelectric barriers: Prediction of four resistance states from first principles, *Nano Lett.* **9**, 427 (2009).
- [59] F.-N. Wang, J.-C. Li, Y. Li, X.-M. Zhang, X.-J. Wang, Y.-F. Chen, J. Liu, C.-L. Wang, M.-L. Zhao, and L.-M. Mei, Prediction of high-mobility two-dimensional electron gas at KTaO_3 -based heterointerfaces, *Chin. Phys. B* **28**, 047101 (2019).
- [60] É. D. Murray and D. Vanderbilt, Theoretical investigation of polarization-compensated II-IV/I-V perovskite superlattices, *Phys. Rev. B* **79**, 100102 (2009).
- [61] M. K. Niranjan, Y. Wang, S. S. Jaswal, and E. Y. Tsymlal, Prediction of a switchable two-dimensional electron gas at ferroelectric oxide interfaces, *Phys. Rev. Lett.* **103**, 016804 (2009).
- [62] N. C. Bristowe, E. Artacho, and P. B. Littlewood, Oxide superlattices with alternating p and n interfaces, *Phys. Rev. B* **80**, 045425 (2009).
- [63] Y. Wang, M. K. Niranjan, S. S. Jaswal, and E. Y. Tsymlal, First-principles studies of a two-dimensional electron gas at the interface in ferroelectric oxide heterostructures, *Phys. Rev. B* **80**, 165130 (2009).
- [64] M. Stengel and D. Vanderbilt, Berry-phase theory of polar discontinuities at oxide-oxide interfaces, *Phys. Rev. B* **80**, 241103 (2009).
- [65] H. Das, N. A. Spaldin, U. V. Waghmare, and T. Saha-Dasgupta, Chemical control of polar behavior in bicomponent short-period superlattices, *Phys. Rev. B* **81**, 235112 (2010).
- [66] V. R. Cooper, Enhanced carrier mobilities in two-dimensional electron gases at III-III/I-V oxide heterostructure interfaces, *Phys. Rev. B* **85**, 235109 (2012).
- [67] P. García-Fernández, P. Aguado-Puente, and J. Junquera, Lattice screening of the polar catastrophe and hidden in-plane polarization in $\text{KNbO}_3/\text{BaTiO}_3$ interfaces, *Phys. Rev. B* **87**, 085305 (2013).
- [68] C. Chen, L. Fang, J. Zhang, G. Zhao, and W. Ren, Thickness control of the spin-polarized two-dimensional electron gas in $\text{LaAlO}_3/\text{BaTiO}_3$ superlattices, *Sci. Rep.* **8**, 467 (2018).
- [69] G. Li, H. Huang, S. Peng, Y. Xiong, Y. Xiao, S. Yan, Y. Cao, M. Tang, and Z. Li, Two-dimensional polar metals in $\text{KNbO}_3/\text{BaTiO}_3$ superlattices: first-principle calculations, *RSC Adv.* **9**, 35499 (2019).
- [70] L. Fang, C. Chen, Y. Yang, Y. Wu, T. Hu, G. Zhao, Q. Zhu, and W. Ren, First-principles studies of a two-dimensional electron gas at the interface of polar/polar $\text{LaAlO}_3/\text{KNbO}_3$ superlattices, *Phys. Chem. Chem. Phys.* **21**, 8046 (2019).
- [71] H. Das, U. V. Waghmare, and T. Saha-Dasgupta, Piezoelectrics by design: A route through short-period perovskite superlattices, *J. Appl. Phys.* **109**, 066107 (2011).
- [72] Z. Zhu, First-principles study of polarization and piezoelectricity behavior in tetragonal PbTiO_3 -based superlattices, *Chin. Phys. B* **27**, 027701 (2018).
- [73] S.-E. Park and T. R. Shrout, Ultrahigh strain and piezoelectric behavior in relaxor based ferroelectric single crystals, *J. Appl. Phys.* **82**, 1804 (1997).
- [74] R. Guo, L. E. Cross, S.-E. Park, B. Noheda, D. E. Cox, and G. Shirane, Origin of the high piezoelectric response in $\text{PbZr}_{1-x}\text{Ti}_x\text{O}_3$, *Phys. Rev. Lett.* **84**, 5423 (2000).
- [75] X. Gonze, J.-M. Beuken, R. Caracas, F. Detraux, M. Fuchs, G.-M. Rignanese, L. Sindic, M. Verstraete, G. Zerah, F. Jollet, M. Torrent, A. Roy, M. Mikami, P. Ghosez, J.-Y. Raty, and D. C. Allan, First-principles computation of material properties: the ABINIT software project, *Comput. Mater. Sci.* **25**, 478 (2002).
- [76] A. M. Rappe, K. M. Rabe, E. Kaxiras, and J. D. Joannopoulos, Optimized pseudopotentials, *Phys. Rev. B* **41**, 1227 (1990).
- [77] A. I. Lebedev, Ab initio calculations of phonon spectra in ATiO_3 perovskite crystals ($A = \text{Ca}, \text{Sr}, \text{Ba}, \text{Ra}, \text{Cd}, \text{Zn}, \text{Mg}, \text{Ge}, \text{Sn}, \text{Pb}$), *Phys. Solid State* **51**, 362 (2009).
- [78] A. I. Lebedev, Phase transitions and metastable states in stressed SrTiO_3 films, *Phys. Solid State* **58**, 300 (2016).
- [79] R. Yu and H. Krakauer, First-principles determination of chain-structure instability in KNbO_3 , *Phys. Rev. Lett.* **74**, 4067 (1995).
- [80] When numbering irreducible representations in this paper, we follow their classification accepted at Bilbao Crystallographic Server [86].
- [81] N. A. Pertsev, A. G. Zembilgotov, and A. K. Tagantsev, Effect of mechanical boundary conditions on phase diagrams of epitaxial ferroelectric thin films, *Phys. Rev. Lett.* **80**, 1988 (1998).
- [82] O. Diéguez, S. Tinte, A. Antons, C. Bungaro, J. B. Neaton, K. M. Rabe, and D. Vanderbilt, Ab initio study of the phase diagram of epitaxial BaTiO_3 , *Phys. Rev. B* **69**, 212101 (2004).
- [83] The periodicity of a superlattice assumes that the electric field strengths \mathcal{E}_1 and \mathcal{E}_2 in its layers satisfy the condition $\mathcal{E}_1 x_1 + \mathcal{E}_2 x_2 = 0$, where x_1 and x_2 are the thicknesses of individual layers. This condition, combined with the equation $(P_1 + \epsilon_1 \mathcal{E}_1) - (P_2 + \epsilon_2 \mathcal{E}_2) = \Delta P$, where P_1 , P_2 , ϵ_1 , and ϵ_2 are spontaneous polarizations and dielectric constants of two layers, gives a solution to this problem in the linear approximation. Solving a nonlinear problem requires more complex calculations.
- [84] R. Resta and D. Vanderbilt, Theory of polarization: A modern approach, in

Physics of Ferroelectrics. A Modern Perspective, edited by K. M. Rabe, C. H. Ahn, and J.-M. Triscone (Springer-Verlag Berlin Heidelberg, 2007) pp. 31–68.

- [85] Z.-Y. Zhu, S.-Q. Wang, and Y.-M. Fu, First-principles study of properties of strained $\text{PbTiO}_3/\text{KTaO}_3$ superlattice, *Chin. Phys. Lett.* **33**, 026302 (2016).
- [86] Bilbao crystallographic server,
<http://www.cryst.ehu.es/>.